ASSESMENT OF THERMAL DISSIPATION EFFECTS IN A VENTRICULAR ASSIST DEVICE

Arunvel Kailasan, Alexandrina Untaroiu, Swapnil Pravin, Houston G. Wood
University of Virginia, Department of Mechanical and Aerospace Engineering
122 Engineer's Way, Charlottesville, VA 22904

ABSTRACT

The heat generated during normal operation of an implantable Left Ventricular Assist Device (LVAD) can have a deleterious effect on the surrounding tissue as well as the blood flowing through the device. This effect is often overlooked and might also result in heart pump failure. Therefore, for a comprehensive design evaluation it is essential to accurately model the thermal dissipation in a LVAD system to ensure safety and device reliability. The *LifeFlow* artificial heart pump is a magnetically suspended axial flow LVAD in which the motor as well as the suspension system are the primary sources for heat generation. The objective of this study is to perform a thorough thermal analysis of the device using a combination of heat transfer equations, 3D-Finite Element analysis and 3D-CFD modeling. Particularly, the effects of heat generated on blood passing through the device due to the motor, magnetic suspension system and housing are studied. Conduction and convection effects due to the above contributors are analyzed. In addition, temperature distributions are estimated for different flow rates and pressure differentials. As a result of this study, it can be inferred if nominal operation of the LifeFlow LVAD would have any significant thermal effects on blood passing through the device. Results show that there is a 2.2°C temperature increase in the magnetic suspension system during nominal operation, while the blood temperature is increasing by 1.6°C. Assessment of thermal effects is crucial since high temperature exposure of blood could ultimately affect the patient whose systemic circulation is supported by the LVAD.

Keywords: thermal analysis, blood, LVAD, heart pump, CFD, FEA, magnetic bearings

Nomenclature

β	Maximum flux density
c	Specific heat
C_D	Skin friction coefficient
C_{motor}	Motor constant
D	Diameter of the fluid region
f	Frequency
h_{local}	Local coefficient of convection
k	Thermal conductivity
L	Thermal region length
Nu_{local}	Local Nusselt number
ŋ	Overall efficiency
$ŋ_{fluid}$	Pump fluid efficiency
$ŋ_{motor}$	Motor efficiency
ρ	Density
P_e	Eddy current losses per unit volume
P_h	Pump head
P_{hy}	Hysteresis loss per unit volume
Pr	Prandtl number
ρ_r	Material resistivity
ΔP_{min}	Minimum pressure head
ΔP_{max}	Maximum pressure head
ΔP_{nom}	Nominal pressure head
Q_{min}	Minimum flow rate
Q_{max}	Maximum flow rate
Q_{nom}	Nominal flow rate
q_{loss}	Heat loss in motor
Re	Reynolds number
r	Rotor Radius
t	Lamination material thickness
τ	Rotor torque
μ	Kinematic Viscosity
v_{mean}	Mean fluid velocity

ω_{min}	Minimum operating speed
ω_{max}	Maximum operating speed
ω_{nom}	Nominal operating speed
λ	Rotor length
ϕ	Radial gap between rotor and stator
ζ	Material constant
ξ	Coefficient related to the geometric structure

INTRODUCTION

Heart failure is one of the leading causes of death in the world with over 20 million people affected and an additional 2 million new patients diagnosed annually [1]. A cardiac transplant is the typical treatment for patients with end stage heart failure, but literature show that shortage of donor hearts available to such patients is a real problem. In the US alone, it is estimated that about 3,100 people are on the waiting list for a cardiac transplant on any given day, with only 2,200 donor hearts available each year [2]. Mechanical heart pumps (left-ventricular and biventricular assist devices) are approved to operate as a "bridge to transplant" device in patients on the waiting list and as a "destination therapy" for patients who are not candidates for a transplant [3-5].

A Ventricular Assist Device (VAD) typically comprises of an impeller, suspension system (mechanical or magnetic bearings), and the motor [6]. Since VADs are designed to be implanted surgically, the heat dissipated to the blood and surrounding tissues must be known. Previous studies have indicated that a temperature rise of 4°C to 6 °C from the body temperature can cause tissue damage along with impairing wound healing and immune response [7]. In addition, it has been reported that tissue necrosis occurs at temperatures above 42°C[8, 9]. The main sources of heat generation during nominal VAD operation are the motor windings and the magnets, either active or passive. Heat generated is absorbed by the housing and is eventually transmitted to the blood and the nearby tissues [10].

The *LifeFlow*™ Left Ventricle Assist Device (LVAD) is a magnetically suspended axial heart pump developed by the University of Virginia [6, 11]. As shown in Figure 1, it comprises of a small, bladed impeller rotated to propel blood through the device. Two sets of stationary blades on the housing are used to increase the efficiency of the pump. The inducer axially directs the blood entering the device. The diffuser converts highly rotational blood coming off the impeller and straightens it translating the circumferential component of the flow into pressure head. The magnetic suspension levitates the impeller and keeps it from contacting the pump wall while it rotates. This is accomplished using arrays of electromagnets called magnetic bearings that attract metal targets located in the impeller. Permanent magnets are also used to keep the impeller centered. The outer housing includes two channels that are designed to accommodate wires from the motor, axial position sensor, and one of the magnetic bearings. This allows all of the wires to exit on the inlet side of the device in a manner that is intended to provide a longer tunneling length for the driveline. Several spacing components are included in the design to ensure proper location and stability of the magnetic suspension and motor assemblies. The inner blood

contacting surfaces are designed so that the seams between them will be compressed as the outer housing is screwed together. This minimizes the risk of thrombus formation in the cracks between components.

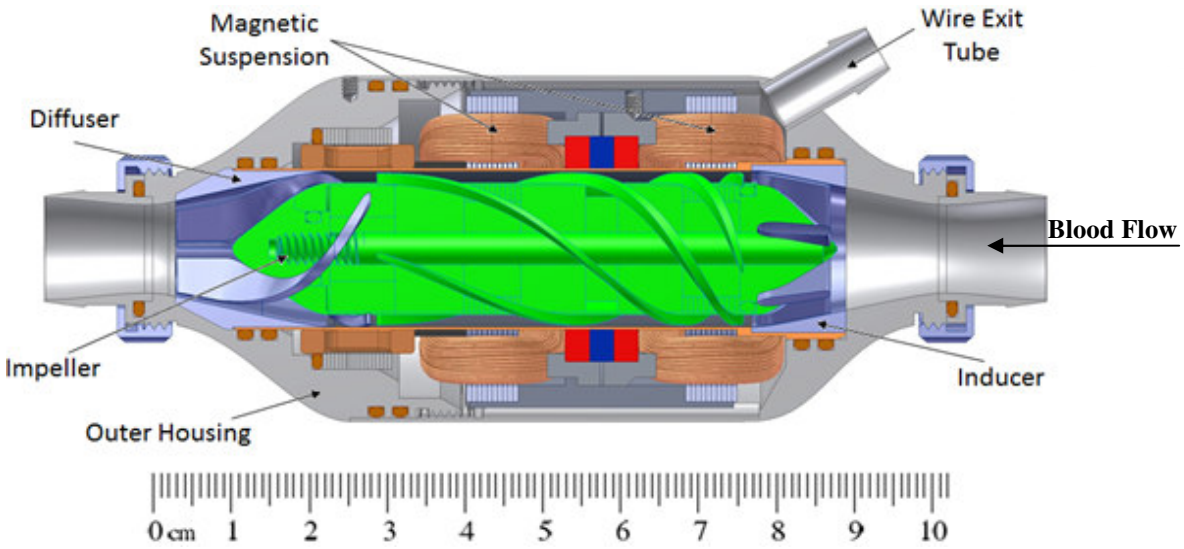

Figure 1. An overview of the LifeFlow Heart Pump with the magnetic suspension system

The primary objective of this study is to better understand the heat effects of the motor and magnetic suspension system on the pump. Initially, the local coefficient of convection at different regions of blood flowing through the pump is calculated. Using these values, the magnetic suspension nominal operating conditions are simulated in 3-D using Autodesk Inventor and the thermal effects on the housing are studied using finite element analysis techniques in ANSYS. This provides a good insight in identifying the main heat sources of the system. Further, a transient heat analysis is performed for the operating conditions in order to study how the heat generated acts with time. The heat losses dissipated by the motor and permanent magnets are calculated. Temperature distribution curves are plotted at different flow rates and operating speeds. Using data from the above studies, the 3D blood flow path is modeled using computational fluid dynamics (CFD). The purpose of this model is to visually analyze how heat from the magnetic suspension is being dissipated onto blood.

MATERIALS AND METHODS

Design Characteristics

The design characteristics of the LifeFlow LVAD are shown in Table 1. The fluid entrance and exit region dimensions are designed to be 11mm in order to fit a cannula which ensures practical implantation [12]. The *LifeFlow* has a minimum (Q_{min}) and maximum (Q_{max}) flow rate of 2 l/min and 8 l/min, with a nominal flow rate (Q_{nom}) of 5 l/min. The design pressure head (ΔP) ranges between 25 mmHg and 180 mmHg. Finally the pump operating speed (ω) ranges from 5000rpm (ω_{min}) to 8000 rpm (ω_{max}) with a nominal speed value of 6000 rpm (ω_{nom}). Titanium alloy

(Ti6Al4V) (k= 6.7 W/m-K) is selected as the housing material due to its superior biocompatibility. A thermally conductive epoxy with low viscosity (k = 0.61 W/m-K) is chosen to act as a heat damper which would help reduce the heat dissipated to surrounding blood and tissue. Blood is assumed and modeled as a Newtonian fluid at body temperature with parameters described in Table 2.

Table 1. Design parameters of LifeFlow VAD

Design Parameter	Value
Minimum Flow rate (Q_{min})	2 L/min
Maximum Flow rate (Q_{max})	8 L/min
Nominal Flow rate (Q_{nom})	5 L/min
Minimum pressure head (ΔP_{min})	25 mmHg
Maximum pressure head (ΔP_{max})	180 mmHg
Minimum operating speed (ω_{min})	5000 rpm
Maximum operating speed (ω_{max})	8000 rpm
Nominal operating speed (ω_{nom})	6000 rpm

Table 2. Modeled properties of blo***od***

Properties	Value
Type	Newtonian
Density (ρ)	1080 kg/m^3
Viscosity (μ)	0.0035 Pa-s
Thermal Conductivity (k)	0.5 W/m-K
Specific heat (c)	3.66 KJ/Kg-K

Solid Part Modeling

A three dimensional thermal model of the LifeFlow LVAD was first created in Autodesk Inventor. This model is then imported into ANSYS 14 for the finite element analysis and a steady state thermal analysis was performed. In order to specify the corresponding boundary conditions associated with the problem, a preliminary calculation was performed to estimate the motor heat loss. The heat loss in a motor can be computed using

$$q_{loss} = \left(QP_h \Big/ \omega C_{motor} \eta_{fluid} \right)^2 \tag{1}$$

where Q is the nominal flow rate, P_h is the pump head, and ω is the operating speed. From Eq.1 it can be deduced that the heat loss in the motor can be computed if the overall efficiency is known. From theory, we know that the overall efficiency [13, 14] is given by

$$\eta = \eta_{motor} \eta_{fluid} = QP_h \Big/ q_{loss} + \tau\omega \tag{2}$$

where motor efficiency is $\eta_{motor} = \tau\omega \Big/ q_{loss} + \tau\omega$ and τ is rotor torque. A motor efficiency of 80% was assumed in order to compute the heat loss. A similar technique was used to study the loss generated by the permanent magnets. The empirical formula expressing the hysteresis loss per unit volume (P_{hy}) is given by Steinmetz [15, 16] as follows

$$P_{hy} = \zeta B^{1.9} f \tag{3}$$

where ζ is the material constant, β represents maximum flux density, and f is the frequency. The eddy current losses, referring to circulating electric currents that are induced in a sheet of conducting material when it is subjected to an alternating magnetic field, are then calculated.

These eddy currents produce power that is dissipated as heat. Assuming that the inductive effects can be neglected, the eddy current losses per unit volume (P_e) [15, 16] can be computed as

$$P_e = {(\pi\beta t f)^2}/{\rho_r \xi} \tag{4}$$

where t is lamination material thickness, ρ_r represents the resistivity of the material and ξ is the coefficient related to the geometric structure.

Windage loss, representing the heat generated in the fluid due to the relative shearing motion of the fluid that flows between the rotor and stator, is then computed. This loss is a function of shaft rotational speed and fluid properties such as temperature, pressure, density and temperature gradients at the stator and rotor walls. A good initial estimate of windage can be given by

$$W = C_D \pi \rho \omega^2 r^4 \lambda \tag{5}$$

$$\mathrm{Re} = {\omega r \phi \rho}/{\mu} \tag{6}$$

where C_D is the skin friction coefficient, r is rotor radius, λ is rotor length and ϕ is the radial gap between rotor and stator.

Based on Eqs. 1-6 the boundary conditions were specified into the model. The computed parameters are shown in Table 3 . The magnetic suspension model and the generated mesh are illustrated in Figure 2 and 3.

Table 3. Summary of losses at operating speed of 6000 rpm

Calculated Loss Parameters	Value
Total Stator Loss	2 W
Copper Loss	1.1 W
Iron Loss	0.9 W
Total Rotor Loss	2.7 W
Shaft Loss	0.4 W
PM loss	2.3 W
Windage Loss	0.7 W
Total Loss (Stator+Rotor+Windage)	5.4 W

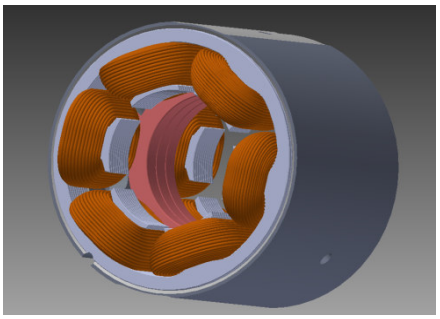

Figure 2. Model of the LifeFlow magnetic suspension system

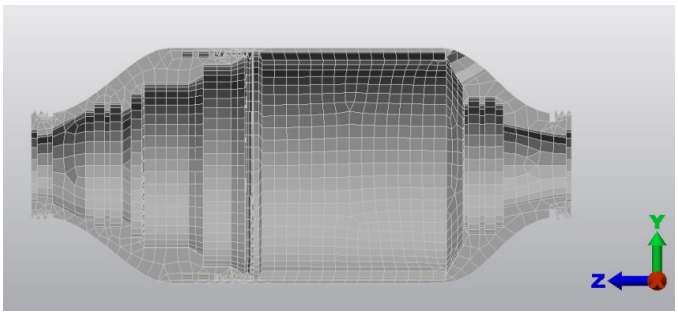

Figure 3 Computational model of the housing

Fluid Modeling

From a fluid flow perspective, a 3D CFD model of the blood flow path was simulated in ANSYS-CFX to study the heat dissipation effects on blood [11, 17, 18]. To facilitate this numerical modeling, results from the solid model, such as surface temperature, stator and rotor losses, and thermal dependence on operating speed and flow rate were utilized. In order to define the fluid model it is vital to compute the corresponding local coefficient of convection, h. From theory, we can compute the Reynolds number [13] as

$$\mathrm{Re}_{region} = \rho v_{mean} D \Big/ \mu \tag{7}$$

where ρ is fluid density, v_{mean} is mean fluid velocity, D is the diameter of the region, and μ is fluid viscosity. The mean fluid velocity can be computed as

$$v_{mean} = 4Q_{nom} \Big/ \pi D^2 \tag{8}$$

The properties of blood are summarized in Table 2. The ratio of the momentum diffusivity to the thermal diffusivity is assumed to be constant and is given by the Prandtl Number

$$\mathrm{Pr} = c\mu \Big/ k \tag{9}$$

From Hausen's correlation, the local Nusselt numbers can then be calculated as

$$Nu_{local} = 3.66 + \frac{0.0668\,\alpha\,\mathrm{Re}\,\mathrm{Pr}}{1 + 0.04(\alpha\,\mathrm{Re}\,\mathrm{Pr})^{2/3}} \tag{10}$$

where $\alpha = D \Big/ L$ and L is the thermal region length. Finally, the local coefficient of convection [19] can be written as

$$h_{local} = Nu_{local} k \Big/ D \tag{11}$$

Based on Eq.11, the local coefficient of convection was recorded at different axial positions within the pump and values are summarized in Table 4. The 3D-CFD model representing the blood flow path is illustrated in Figure 4. A mesh convergence study resulted in a model with approx. 900 thousand elements. The pump operating condition of 5L/min and a rotor speed 6,000 rpm [11, 12] was simulated using ANSYS-CFX.

Table 4. Calculated convection values

Axial Distance from entrance (cm)	Convection values (h) W/m^{2}K
0 (inlet)	1,800
2	2,200
4	4,300
6	7,100
8	8,900
10	2,400
12 (outlet)	1,800

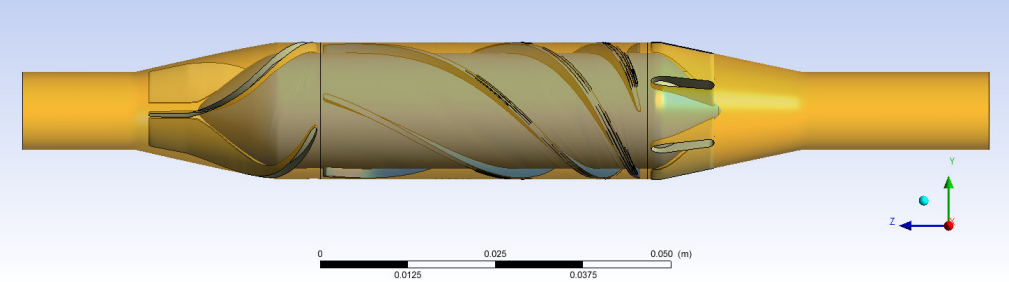

Figure 4. CFD model of blood flow path

RESULTS AND DISCUSSION

The solid model described in the section above was solved first to calculate the temperature distribution profile. Results were then input as boundary conditions for the 3D fluid part model of the pump. Subsequently, the temperature dependence on various parameters such as flow rate, operational speed and pressure head was calculated.

Solid Model and Temperature Distribution

In order to solve the solid model, the boundary conditions described in the section above were prescribed. The heat loss values calculated were input as a load into the model. To perform a steady state heat analysis, a flow of 5L/min at a pressure head of 81.8 mmHg was set. Based on a mesh convergence study, a computational model comprising of approx. 300,000 elements was selected and utilized in the analysis. Figure 5 shows the temperature distribution profile as obtained from Ansys 14 simulation software. It should be noted that Figure 5 shows the heat conducted onto the titanium housing of the pump. From the figure, it can be deduced that the highest temperatures were obtained at locations near the magnetic suspension system. The maximum temperature obtained was roughly at the middle of the pump and was about 39.3°C (102.74 F) - a 2.3°C rise from the body temperature. An interesting observation is that the heat from the magnetic suspension does not conduct very fast to the surrounding areas of the pump. This is thought to be due to the epoxy coating on the suspension.

A transient heat analysis was also performed to visualize the temperature increase with time. To reduce the computational time, three points of interest were selected using the probe tool and the temperature at each of these points was recorded at a particular time. Monitor points were set at the inducer side, diffuser side and the mid-point of the magnetic suspension system, as shown in Figure 6. The temperature at each of these points was recorded for 600 seconds and the results are plotted in Figure 7. It can be seen that the temperature rise in the inducer and diffuser are almost similar. The very slight temperature increase at the diffuser side can be attributed to the heat dissipation from the magnetic suspension system. An interesting point to be observed here is that most of the temperature rise occurs within the first 200 seconds of operation. At the magnetic suspension, there is a steep rise of 2.25°C within this time while the other areas show an increase of 0.5°C.

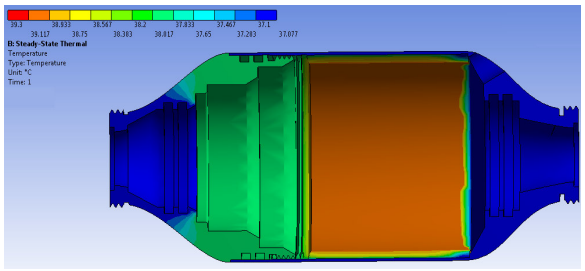

Figure 5. Contour plot of temperature

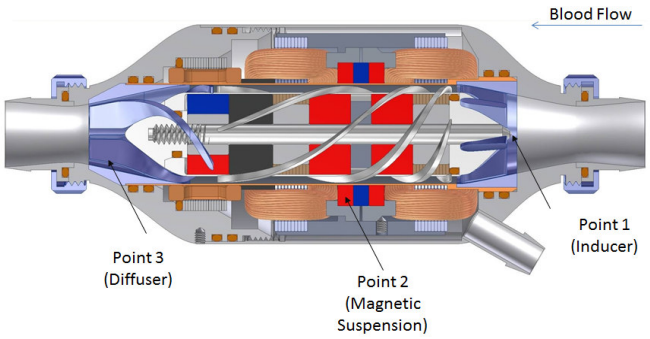

Figure 6. Monitor points for transient heat analysis

The temperature distribution of the entire pump was observed after 180 seconds at a flow rate of 5L/min and at a pressure head of 81.8 mmHg. This curve is depicted in Figure 8. The x –axis shows the normalized axial distance, where 0 indicates the inlet and 1 the outlet.

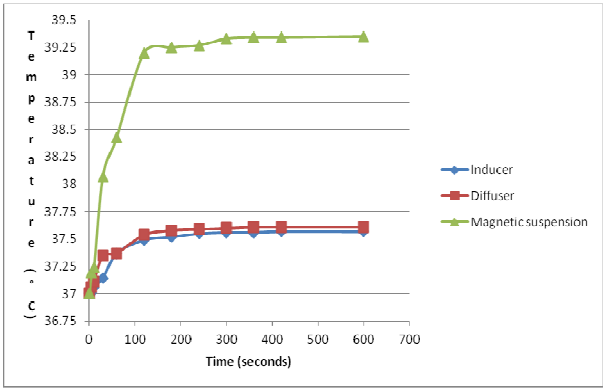

Figure 7. Temperature distribution vs. time

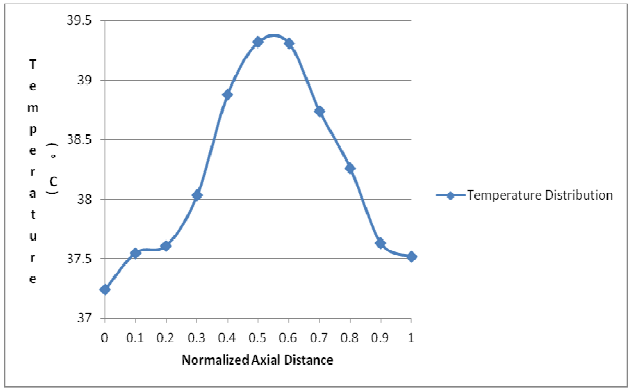

Figure 8. Temperature vs. Normalized axial distance

It can be noted that the highest temperature occurs at the mid-point of the pump where the magnetic suspension system is located. A maximum temperature of 39.4°C was observed at this point. The outlet temperature is slightly higher than the inlet temperature. This is thought to be due to the conduction effects of the magnetic suspension.

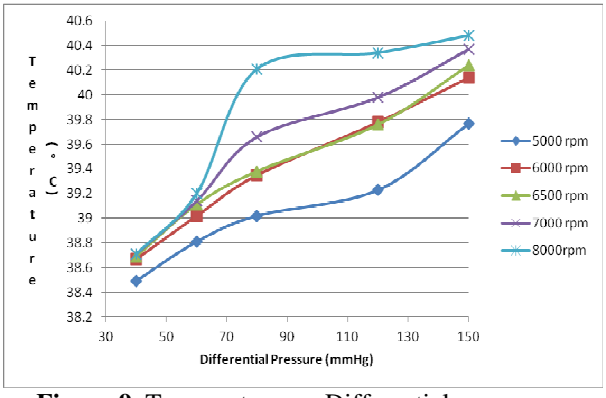

Figure 9. Temperature vs. Differential pressure for different operating speeds

The maximum temperature corresponding to different operating speeds and pressure heads were also calculated and are shown in Figure 9. As anticipated, an increase in differential pressure leads to a slight increase in temperature. A maximum temperature of 40.4°C was calculated for an operating speed of 8,000 rpm and a differential pressure of 150mmHg. The study was conducted at a nominal flow rate of 5L/min.

Fluid Model

As indicated previously, to visualize the thermal effects of the magnetic suspension on blood, a 3D model of the flow path was modeled in ANSYS-CFX. The temperature distribution results from the solid model were used as the wall temperature input into the fluid model. The case of a flow rate of 5L/min and a rotating speed for 6,000 rpm was analyzed. Figure 10 shows the temperature distribution as observed on blood. It can be seen that the inlet temperature is set at 37°C. As the blood crosses the inducer and reaches the magnetic suspension area, the temperature starts to increase. Even though a 2.25°C increase was observed in the solid model described above, an increase of about 1.5°C was noticed in the modeled blood temperature. This is thought to be due of the constant flow of blood through the pump. As blood moves away from this heat source, it cools down to about 37.8°C at the diffuser region– an increase of 0.8°C from the inlet. Due to thermal conductivity of blood, heat is quickly dissipated. The results obtained from the fluid model correspond well with that obtained from the solid model. The maximum temperature increase was about 1.6°C which is well within the safe range (+3°C) as suggested in the literature.

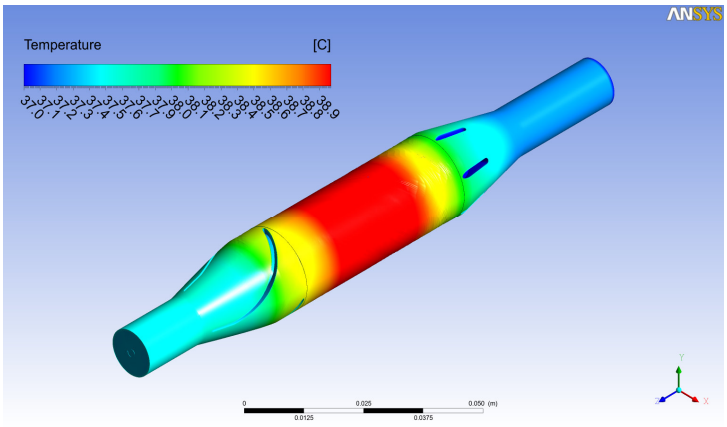

Figure 10. Blood Temperature distribution

CONCLUSION

The main objective of this study is to analyze the thermal effects of the LifeFlow LVAD during nominal operation. The problem was divided between a solid and a fluid model. First of all, the heat generated by the magnetic suspension system is analyzed using mathematical models and FE analysis. At the nominal operating speed of 6000 rpm and a flow rate of 5L/min, it was found that the temperature of the LVAD section would increase by approximately 2.4°C. From the study it is also clear that the magnetic suspension system is the main source of heat generation in the pump. A transient heat analysis was performed to study how the temperature rises with time. It was observed that after a time period of 200 seconds, the temperature flattened out. Temperature distribution curves were plotted at different pressure levels and operating speeds. From literature it is understood that a temperature rise of 4°C- 5°C could cause severe tissue and blood damage [7]. The LifeFlow LVAD's temperature profile indicates that even at extreme operating conditions, the temperature rise is well below this value. Finally, a 3D model was used to analyze the heating effects on blood. The wall temperature boundary conditions were input from the solid model. The temperature distribution was plotted for a flow rate of 5L/min and an operating condition of 6000 rpm. A temperature rise of 2.2°C was observed from the solid model while a rise of about 1.6°C was seen in the fluid model. These initial studies show that blood

flowing through the LifeFlow LVAD will not be significantly affected by the heat generated by system components when device is operating at the nominal conditions selected.

REFERENCES

[1] Lloyd-Jones, D., Adams, R. J., Brown, T. M., 2010, "Heart Disease and Stroke statistics—2010 Update," Circulation, **121**(7) pp. e46-e215.
[2] Hassinger, M. P., 2012, "Total Artificial Heart Freedom Driver in a Patient with End-Stage Biventricular Heart Failure," AANA Journal, **80**(2) pp. 105.
[3] Birks, E. J., Tansley, P. D., Hardy, J., 2006, "Left Ventricular Assist Device and Drug Therapy for the Reversal of Heart Failure," New England Journal of Medicine, **355**(18) pp. 1873-1884.
[4] Frazier, O., Myers, T. J., Westaby, S., 2003, "Use of the Jarvik 2000 Left Ventricular Assist System as a Bridge to Heart Transplantation Or as Destination Therapy for Patients with Chronic Heart Failure," Annals of Surgery, **237**(5) pp. 631.
[5] Park, S. J., Tector, A., Piccioni, W., 2005, "Left Ventricular Assist Devices as Destination Therapy: A New Look at Survival," J Thorac Cardiovasc Surg, **129**(1) pp. 9-17.
[6] Kailasan, A., Untaroiu, A., Jiang, W., 2012, "Lifeflow Vad: Design and Numerical Modeling of Magnetic Bearing System," Biomedical Sciences Instrumentation, **48**pp. 218-225.
[7] Okazaki, Y., Davies, C. R., Matsuyoshi, T., 1997, "Heat from an Implanted Power Source is mainly Dissipated by Blood Perfusion." ASAIO Journal (American Society for Artificial Internal Organs: 1992), **43**(5) pp. M585.
[8] Yamazaki, K., Litwak, P., Kormos, R. L., 1997, "An Implantable Centrifugal Blood Pump for Long Term Circulatory Support." ASAIO Journal (American Society for Artificial Internal Organs: 1992), **43**(5) pp. M686.
[9] Seese, T., Harasaki, H., Saidel, G., 1998, "Characterization of Tissue Morphology, Angiogenesis, and Temperature in the Adaptive Response of Muscle Tissue to Chronic Heating," Laboratory Investigation, **78**,pp. 1553-1562.
[10] Navarro, R. R., Kiraly, R. J., Harasaki, H., 1988, "Heat Dissipation through the Blood Contacting Surface of a Thermally Driven LVAS," The International Journal of Artificial Organs, **11**(5) pp. 381-386.
[11] Untaroiu, A., Wood, H. G., Allaire, P. E., 2005, "Computational Design and Experimental Testing of a Novel Axial Flow LVAD," ASAIO Journal, **51**(6) pp. 702-710.
[12] Untaroiu, A., Throckmorton, A. L., Patel, S. M., 2005, "Numerical and Experimental Analysis of an Axial Flow Left Ventricular Assist Device: The Influence of the Diffuser on overall Pump Performance," Artificial Organs, **29**(7) pp. 581-591.
[13] Brown, M.E., 2001, "Introduction to thermal analysis: techniques and applications," Springer, .
[14] Gardiner, J. M., Wu, J., Noh, M. D., 2007, "Thermal Analysis of the PediaFlow Pediatric Ventricular Assist Device," ASAIO Journal, **53**(1) pp. 65-73.
[15] Zheng, L., and Acharya, D., 2009, "Losses in High Speed Permanent Magnet Machines used in Microturbine Applications," Journal of Engineering for Gas Turbines and Power, **131**pp. 022301-022301.
[16] Zeisberger, M., and Gawalek, W., 1998, "Losses in Magnetic Bearings," Materials Science and Engineering: B, **53**(1) pp. 193-197.
[17] Song, X., Throckmorton, A. L., Wood, H. G., 2003, "Computational Fluid Dynamics Prediction of Blood Damage in a Centrifugal Pump," Artificial Organs, **27**(10) pp. 938-941.
[18] Throckmorton, A. L., Untaroiu, A., Lim, D. S., 2007, "Fluid Force Predictions and Experimental Measurements for a Magnetically Levitated Pediatric Ventricular Assist Device," Artificial Organs, **31**(5) pp. 359-368.
[19] Busse, F., 2001, "Non-Linear Properties of Thermal Convection," Reports on Progress in Physics, **41**(12) pp. 1929.